Global trends in extremal microseism intensity

Richard C. Aster,[1] Daniel E. McNamara,[2] and Peter D. Bromirski[3]

Received 30 March 2010; revised 25 May 2010; accepted 7 June 2010; published 21 July 2010.

[1] Globally ubiquitous seismic background noise peaks near 7 and 14 s period are generated via distinct mechanisms that transfer storm-generated gravity wave energy to the seismic wave field. We utilize continuous digital ground motion data recorded by the Global Seismographic Network and precursor instrumentation to chronicle microseism power extreme events for 1972–2009. Because most land-observed microseism surface-wave energy is generated at or near coasts, microseism metrics are particularly relevant to assessing changes in coastal ocean wave energy. Extreme microseism winter storm season event counts reveal the widespread influence of the El Niño Southern Oscillation (ENSO). Individual station and ensemble slopes trend positive for this study period for Northern Hemisphere stations. The double-frequency microseism is particularly volatile, suggesting that the weaker single-frequency microseism directly generated by ocean swell at coasts is likely a more representative seismic proxy for broad-scale ocean wave energy estimation.
Citation: Aster, R. C., D. E. McNamara, and P. D. Bromirski (2010), Global trends in extremal microseism intensity, *Geophys. Res. Lett.*, *37*, L14303, doi:10.1029/2010GL043472.

1. Introduction

[2] Ocean wave variability in coastal regions is of fundamental relevance to extreme storm statistics and climate studies [*Levitus et al.*, 2000; *Kunkel et al.*, 2008] and is of great societal concern under rising sea levels. Recent studies have suggested that climate change may affect the frequency, distribution, and/or intensity of storms and associated ocean wave activity, for example in hurricanes affecting the eastern U.S. and Caribbean [*Emanuel*, 2005; *Federov et al.*, 2010], in northern Pacific winter cyclones [e.g., *Graham and Diaz*, 2001; *Bromirski et al.*, 2005a; *Lambert and Fyfe*, 2006], and in extratropical storms affecting northern Europe [e.g., *Grevemeyer et al.*, 2000; *Essen et al.*, 2003]. In this paper, we concentrate on global winter period storms and demonstrate that microseism data from existing Global Seismographic Network (GSN) [*Butler et al.*, 2004] infrastructure provides a valuable real-time metric for comparing extreme coastal wave events across decadal time spans.

[3] Earth's ambient seismic noise spectrum is dominated by broad and dominant peaks near 7 and 14 s period that are principally due to seismic surface waves. This excitation, the microseism, is observed globally, even in deep continental interiors (Figure 1), and has long been recognized as a proxy of ocean wave and storm intensity [*Gutenberg*, 1947]. The single-frequency (SFM; primary) and double-frequency microseism (DFM; secondary) power spectral density peaks are largely unaffected by common anthropogenic noise sources [*Withers et al.*, 1996; *McNamara and Buland*, 2004]. SFMs are generated at the causative ocean swell period via direct pressure fluctuations at the ocean bottom in shallow water resulting from breaking and/or shoaling waves [*Hasselmann*, 1963]. The amplitude of the much stronger DFM is proportional to the square of standing-wave components of the ocean wave field [*Longuett-Higgins*, 1950], such as where incoming swell interacts with coastal reflections [*Bromirski et al.*, 1999]. Intense cyclonic low-pressure storm systems have steep pressure gradients that cause strong surface winds that transfer atmospheric energy into ocean swell [*Pierson and Moskowitz*, 1964], and subsequently into microseism energy. The seasonal distribution of ocean wave energy and its long-term variability are influenced by broad-scale climate factors [*Bromirski et al.*, 2005a] that are reflected in microseism level variations [*Aster et al.*, 2008].

[4] The spatially integrative character of microseisms arises from both the efficient propagation of ocean swell across ocean basins [*Munk et al.*, 1963; *Bromirski and Duennebier*, 2002; *MacAyeal et al.*, 2006], and from the semi-coherent impact of swell along long stretches of coastline [*Bromirski et al.*, 2005b; *Aster et al.*, 2008]. Microseism metrics from global networks of long-running calibrated seismic stations are thus an integrative complement to other wave intensity monitors such as ocean buoys [*Bromirski and Duennebier*, 2002; *Aster et al.*, 2008] and iceberg- or iceshelf-deployed seismometers [*MacAyeal et al.*, 2006; *Bromirski et al.*, 2010]. Because most microseism energy observed on land is coastally generated [*Bromirski et al.*, 1999; *Bromirski*, 2001; *Bromirski and Duennebier*, 2002; *Gerstoft and Tanimoto*, 2007], extremes in microseism energy strongly correlate with extremes in near-shore wave energy [e.g., *Aster et al.*, 2008].

2. Data Analysis

[5] We analyze microseism power using continuous 1 sample/s digital vertical-component time series from the GSN and predecessor networks at sites selected solely for long continuous recording history and wide geographic distribution (Figure 1 and Table S1 of the auxiliary material).[4] Secular variations in winter storm season extreme microseism power levels are analyzed from 1972–2009. Our methodol-

[1]Department of Earth and Environmental Science, New Mexico Institute of Mining and Technology, Socorro, New Mexico, USA.
[2]U.S. Geological Survey, Denver, Colorado, USA.
[3]Integrative Oceanography Division, Scripps Institution of Oceanography, La Jolla, California, USA.

0094-8276/10/2010GL043472

[4]Auxiliary materials are available in the HTML. doi:10.1029/2010GL043472.

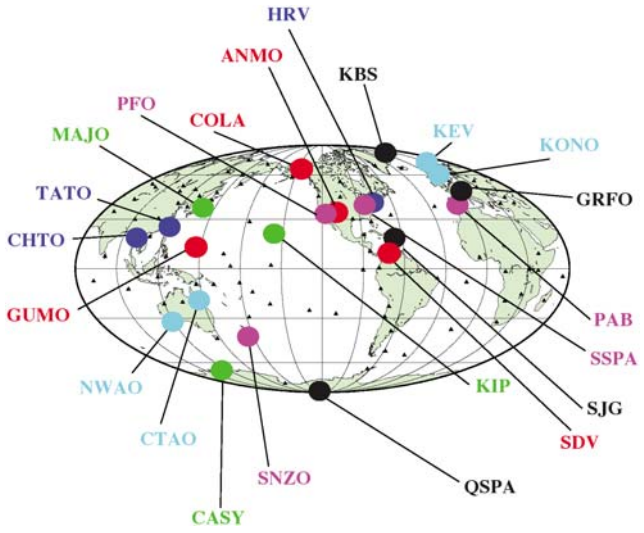

Figure 1. Locations of Global Seismographic Network and predecessor seismic stations analyzed in this study (Table S1).

ogy exploits a comprehensive database of power spectral densities (PSDs) calculated using 50% overlapping 3-hour sections. Each 3-hour PSD is an average of 13 sub-segments, overlapping by 75%, that are smoothed into full-octave averages over 1/8-octave intervals, giving 96 spectral estimates between 2 to 940 s period [*McNamara and Buland*, 2004]. These processing parameters provide suitable temporal and spectral resolution for discriminating between relatively narrow-band, long-term ocean wave events and spectrally broadband, short-term transients from instrumentation malfunctions and earthquakes (Figure S1).

[6] Ocean wave and consequent microseism spectral amplitudes decline rapidly at periods longer than 25 s [*Bromirski et al.*, 1999; *Bromirski and Duennebier*, 2002], but earthquake transients are much more broadband (Figure S1). Earthquake-dominated and microseism-dominated spectra can thus be reliably discriminated via spectral detection. PSDs with frequency bins that are 95% outside of the 1st through the 80th PSD percentiles at periods >30 s (5th through 80th for some earlier stations; Figures S1c and S1d) are removed from further consideration [*McNamara et al.*, 2009] to produce an earthquake-culled data set.

[7] To quantify extreme ocean wave/microseism events, we have developed a short- versus long-term power level ratio detection algorithm and applied it to each microseism band. The DFM band (5–9 s) power level is the average of 9 estimates and the SFM band (14–20 s) power level is the average of 7 estimates across the smoothed and section-averaged PSDs calculated as described above. To reduce possible biases associated with instrument transfer functions, we self-normalize the detection procedure by evaluating percentile statistics relative to the PSD median across long-term instrumentation epochs for which station metadata indicate a non-changing instrument transfer function. This is a conservative correction that generally reduces trends. An ocean wave/microseism event trigger occurs when at least 3 consecutive PSDs (i.e., 6 continuous hours) exceed the 95th percentile of the earthquake-culled dataset. We define "microseism index" as the number of event trigger hours per month, and the total number of such hours detected per year is referred to as annual "index hours" (see the auxiliary material for additional details on data selection criteria, spectral estimation methods, instrumentation bias corrections, and the microseism index algorithm).

[8] Microseism indices were determined for 23 GSN stations restricted to winter months (November–March for the Northern Hemisphere and May–September for the Southern Hemisphere). This allows this study to concentrate on extratropical storms associated with particularly large and geographically extensive swell events. Winter microseism indices were determined for all months with at least 65% total data availability following earthquake and other transient removal. To correct potential influences due to changing data availability or other uptime trends through time, monthly microseism triggers hours were prorated to a full winter period based on uptime.

3. Discussion and Conclusions

[9] The SFM winter storm season microseism index trend for all 23 stations (Figure 1, Table S2, and Figure S4) are suggestive of a widespread upward trend in global coastal wave activity in the northern Hemisphere during this study period in temperate latitudes, (geographic yearly depictions of these results are shown in Figures S2 and S3. Figure S4 shows latitudinal dependencies of SFM and DFM slopes, indicating that the trend, to the extent that it can be generalized, is predominantly observed at northern temperate latitudes (which may be partially an artifact of historical station distribution).

[10] Especially volatile inter-annual behavior is notable at North Atlantic stations (Figures 2, S2, and S3) [*Grevemeyer et al.*, 2000; *Essen et al.*, 2003]. Station-specific, regional, and global linear trends evaluated via L_2-norm regression with bootstrap parameter estimates display a bias for positive regression slopes (Figures 2 and S4). For the SFM, which constitutes the longest available time record, 56% (13) of stations had positive slopes, with 39% (9), 4% (1), and 4% (1) of these being positive at 1, 2, and 3σ significance, respectively. Just 2 (9%) of Southern Hemisphere stations, SNZO (New Zealand), and NWAO (western Australia), had negative regression slopes that were significant at the 1σ or greater significance. 12 stations were indistinguishable from zero linear trend at the 1σ level. Comparable average metrics for the shorter (since 1990) DFM record, in contrast to that of the SFM, show more ambiguous overall slope trends (with larger uncertainties), lower R^2 values (Table S3 and Figures 2 and S4), greater inter-annual variation (Figure S5) and higher average index values indicative of greater inter-annual variation (162 versus 77.8 hr/y). Prior to about the mid-1980s, filtering of the strong secondary microseism peak to accommodate lower dynamic range recording systems precludes analysis of earlier DFM variability (Figures S1c and S1d). Because the coupling mechanism of the SFM results from the ubiquitous semi-coherent breaking and shoaling of ocean waves at coasts while the DFM requires near-surface wave-wave interactions, the differences in peak-to-peak features between the two metrics are likely a consequence of DFM sensitivity to coast- and wave-specific conditions affecting the production of opposing wave components. Continental interior stations tend to show stronger DFM-SFM index

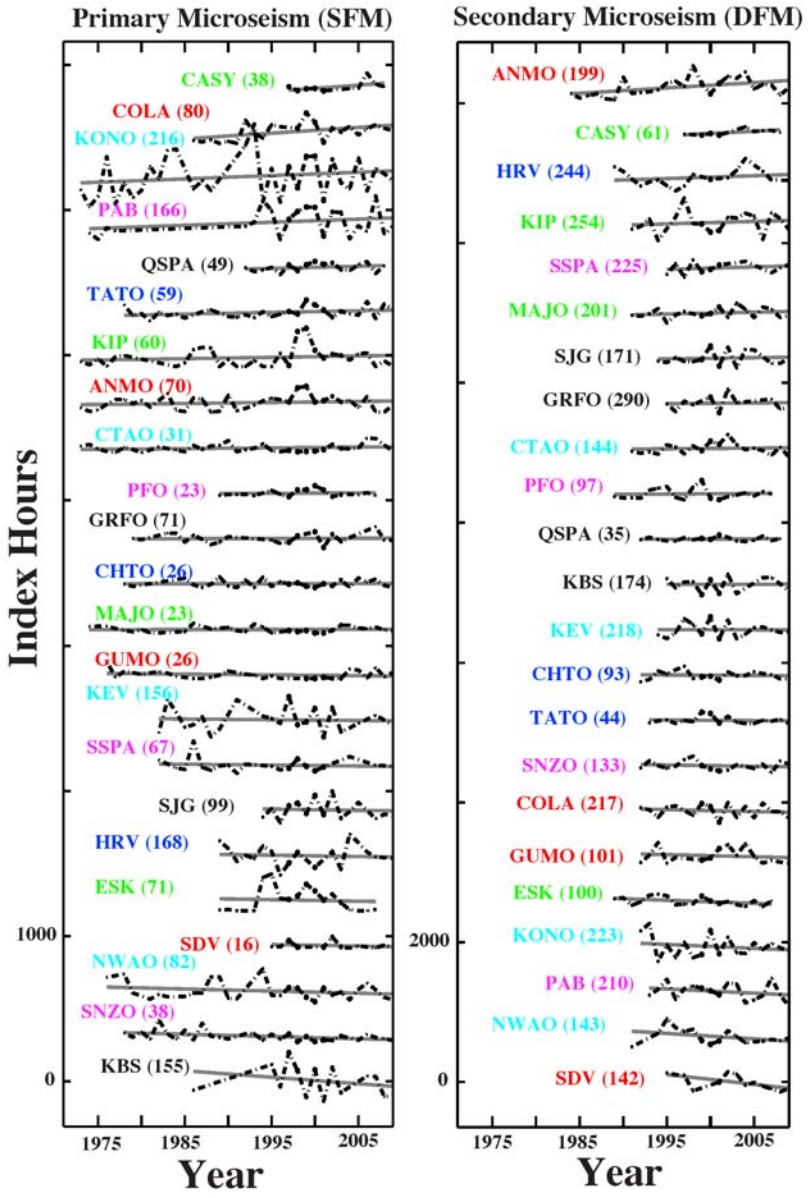

Figure 2. L_2 regression analysis of winter-month annual average 95th percentile microseism index trends for the (left) SFM and (right) DFM for the stations of Figure 1 (Tables S1–S3), sorted by decreasing linear regression slope in each case, with average microseism index hours per year indicated. Because of pre-GSN filtering of the shorter period end of the microseism band, DFM results are only calculable from the mid-1980s and later. Individual station regression results are shown in Table S2 and averaged results and regressions are shown in Figure 3. Respective depictions of yearly departures from means are shown geographically in Figures S2 and S3. Latitudinal slope dependence is shown in Figure S4, and DFM/SFM correlations are displayed in Figure S5.

correlation, while some near-coastal stations (e.g., CTAO, MAJO, KIP, and ESK) show a number of years with excess DFM/SFM anomalies (Figure S5). This DFM "bright spot" effect has been previously noted for northern European stations (e.g., ESK) by *Essen et al.* [2003] and elsewhere, and may be a ubiquitous feature of source regions featuring steep coastlines in stormy regions (e.g., parts of northern Europe, southern Greenland, northwestern North America, and southwestern South America).

[11] SFM index hour maxima in 1978, 1983, 1987 and 1998 occur during moderate and strong El Niño episodes, and also occur during the strong La Niña episodes of 1999 and 2000 (Figures 2 and 3). This is unsurprising, given that ENSO events have a significant effect on the generation, intensity, and steering of Pacific storms, thus affecting the magnitude and distribution of ocean wave energy along coastlines [*Bromirski et al.*, 2005a]. ENSO events are further observed to have an influence on global microseism extrema (Figures S2 and S3). The global and large-scale averaged SFM index regression results (Figure 3), dominated by Northern Hemisphere activity due to the geographic distribution of stations (Figure 1), indicate an increasing global trend in near-coastal ocean wave activity over the past 3–4 decades in the Northern Hemisphere and a stable or slightly declining trend in the Southern Hemisphere (Northern Hemisphere slope: $6.8 \pm 4.3 \cdot 10^{-3}$ y^{-1};

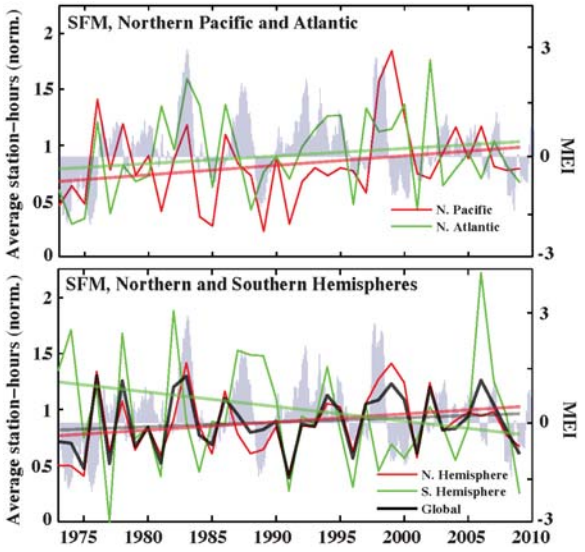

Figure 3. Northern Pacific (ANMO, COLA, GUMO, KIP, MAJO, PFO, TATO) northern Atlantic (ESK, GRFO, HRV, KBS, KEV, KONO, PAB, SDV, SJG, SSPA), and N/S Hemisphere winter season SFM station averages, with each constituent stations normalized by average hours (Figure 1). Multivariate El Niño Index (MEI) monthly determinations (National Center for Atmospheric Research; http://www.cgd.ucar.edu/cas) are shown in blue.

Southern Hemisphere slope: $-9.6 \pm 8.0 \cdot 10^{-3}$ y^{-1}; global slope: $4.0 \pm 8.0 \cdot 10^{-3}$ y^{-1}). SFM results for regional north Pacific- and north Atlantic-affinity stations [*Aster et al.*, 2008] also show positive slopes ($7.9 \pm 4.7 \cdot 10^{-3}$ y^{-1} and $5.9 \pm 5.7 \cdot 10^{-3}$ y^{-1}, respectively). An exceptional spike in Southern Hemisphere SFM, but not DFM, index hours during the 2006 austral winter is coherently observed across southwest Pacific stations (Figures 2 and S2), suggesting, again, that specific storm location and track variations operating on an annual scale direct swell along propagation paths that strongly influence DFM excitation. A notable leveling off in both SFM and DFM annual index hours beginning around 2005 may reflect the recent lack of strong ENSO episodes prior to the El Niño that began in 2009, which has modestly reversed this globally declining trend for the 2009–2010 winter Northern Hemisphere wave year [*Aster et al.*, 2010].

[12] The lower frequency ambient seismic noise SFM band, although typically having spectral levels about 20 dB lower than the DFM component, is more easily extendable to earlier seismographic systems where strong filtering in the DFM period band was commonly employed. Lower frequency SFM surface waves will furthermore propagate to interior continental stations with less attenuation than the DFM. This work further supports the view that differences between the two microseism components reflect increased sensitivity to specific coastal and storm conditions for exciting the standing wave components of the ocean wave field necessary for DFM excitation, although swell directional and other effects must also influence SFM generation to some degree. Because SFM is likely less sensitive to swell incident angle and coastline configuration than DFM, we suggest that the SFM may be a more representative proxy for integrated wave energy impacting coastlines than the DFM, and that interior continental stations (e.g., more than 100 km from coasts (Figure S5)) may ultimately prove to be superior observatories of broad-scale ocean wave state variation over long durations due to superior spatiotemporal integrative characteristics (Figure S5).

[13] Increasing oceanic wave energy has broad implications for coastal impacts, especially under rising sea levels that will allow more wave energy to reach farther shoreward. Additionally, ocean swell and infragravity waves may furthermore play a role the destabilization of ice shelves [*MacAyeal et al.*, 2006; *Bromirski et al.*, 2010]. While ENSO is a natural oscillation of the Earth's climate, an important and timely concern is whether the intensity or occurrence of extreme wave events generated by ENSO- and/or otherwise-influenced storms is increasing.

[14] Ocean wave energy reaching coasts during storm events exhibits considerable variability in amplitude and spatiotemporal distribution, which could be more thoroughly assessed with more complete and continued development of monitoring methods using both historical and modern real-time seismographic data in conjunction with enhanced microseism source modeling and more advanced observation techniques, and in conjunction with oceanographic instrumentation. Because the microseism index method is self-normalized, it is robust in the face of early instrumentation variability and record incompleteness. Thus, digitization and analysis of paper and film records from the analog recording era should facilitate extending this methodology backward, potentially to the early 20th century.

[15] **Acknowledgments.** The Global Seismographic Network is a cooperative scientific facility operated jointly by the Incorporated Research Institutions for Seismology, the United States Geological Survey (USGS), and the National Science Foundation. P. Bromirski was supported in this research by the California Department of Boating and Waterways. Figures were created using MATLAB. Richard Boaz contributed significantly to database programming. We thank USGS colleagues Lind Gee and Adam Ringler, and two external reviewers for helpful comments during review.

References

Aster, R., D. E. McNamara, and P. Bromirski (2008), Multi-decadal climate-induced variability in microseisms, *Seismol. Res. Lett.*, *79*, 194–202.

Aster, R. C., D. E. McNamara, and P. Bromirski (2010), Global trends in microseism intensity from the 1970s to present, *Seismol. Res. Lett.*, *81*, 364.

Bromirski, P. D. (2001), Vibrations from the "Perfect Storm," *Geochem. Geophys. Geosyst.*, *2*, 1030, doi:10.1029/2000GC000119.

Bromirski, P. D., and F. K. Duennebier (2002), The near-coastal microseism spectrum: Spatial and temporal wave climate relationships, *J. Geophys. Res.*, *107*(B8), 2166, doi:10.1029/2001JB000265.

Bromirski, P. D., R. E. Flick, and N. Graham (1999), Ocean wave height determined from inland seismometer data: Implications for investigating wave climate changes in the northeast Pacific, *J. Geophys. Res.*, *104*, 20,753–20,766.

Bromirski, P. D., D. R. Cayan, and R. E. Flick (2005a), Wave spectral energy variability in the northeast Pacific, *J. Geophys. Res.*, *110*, C03005, doi:10.1029/2004JC002398.

Bromirski, P. D., F. K. Duennebier, and R. A. Stephen (2005b), Mid-ocean microseisms, *Geochem. Geophys. Geosyst.*, *6*, Q04009, doi:10.1029/2004GC000768.

Bromirski, P. D., O. V. Sergienko, and D. R. MacAyeal (2010), Transoceanic infragravity waves impacting Antarctic ice shelves, *Geophys. Res. Lett.*, *37*, L02502, doi:10.1029/2009GL041488.

Butler, R., et al. (2004), The Global Seismographic Network surpasses its design goal, *Eos Trans. AGU*, *85*(23), 225, doi:10.1029/2004EO230001.

Emanuel, K. (2005), Increasing destructiveness of tropical cyclones over the past 30 years, *Nature*, *436*, 686–688.

Essen, H.-H., F. Krüger, T. Dahm, and I. Grevemeyer (2003), On the generation of secondary microseisms observed in northern and central Europe, *J. Geophys. Res.*, *108*(B10), 2506, doi:10.1029/2002JB002338.

Federov, A., C. Brierly, and K. Emanuel (2010), Tropical cyclones and permanent El Niño in the early Pliocene epoch, *Nature*, *463*, 1066–1070.

Graham, N. E., and H. F. Diaz (2001), Evidence for intensification of North Pacific winter cyclones since 1948, *Bull. Am. Meteorol. Soc.*, *82*, 1869–1893.

Gerstoft, P., and T. Tanimoto (2007), A year of microseisms in southern California, *Geophys. Res. Lett.*, *34*, L20304, doi:10.1029/2007GL031091.

Grevemeyer, I., R. Herber, and H. Essen (2000), Microseismological evidence for a changing wave climate in the northeast Atlantic Ocean, *Nature*, *408*, 349–352.

Gutenberg, B. (1947), Microseism and weather forecasting, *J. Meteorol.*, *4*, 21–28.

Hasselmann, K. (1963), A statistical analysis of the generation of microsiesms, *Rev. Geophys.*, *1*, 177–209.

Kunkel, K. E., et al. (2008), *Observed Changes in Weather and Climate Extremes in Weather and Climate Extremes in a Changing Climate. Regions of Focus: North America, Hawaii, Caribbean, and U.S. Pacific Islands*, edited by T. R. Karl et al., U.S. Clim. Change Sci. Program, Washington, D. C.

Lambert, S., and J. Fyfe (2006), Changes in winter cyclone frequencies and strengths simulated in enhanced greenhouse gas experiments: Results from the models participating in the IPCC diagnostic exercise, *Clim. Dyn.*, *26*, 713–728.

Levitus, S., J. Antonov, T. Boyer, and C. Stephens (2000), Warming of the world ocean, *Science*, *287*, 2225–2229.

Longuett-Higgins, M. S. (1950), A theory of the origin of microseisms, *Philos. Trans. R. Soc. London A*, *243*, 1–35.

MacAyeal, D. R., et al. (2006), Transoceanic wave propagation links iceberg calving margins of Antarctica with storms in tropics and Northern Hemisphere, *Geophys. Res. Lett.*, *33*, L17502, doi:10.1029/2006GL027235.

McNamara, D., and R. Buland (2004), Ambient noise levels in the continental United States, *Bull. Seismol. Soc. Am.*, *94*, 1517–1527.

McNamara, D. E., C. R. Hutt, L. S. Gee, H. M. Benz, and R. P. Buland (2009), A method to establish seismic noise baselines for automated station assessment, *Seismol. Res. Lett.*, *80*, 628–637.

Munk, W. H., G. Miller, F. Snodgrass, and N. Barber (1963), Directional recording of swell from distant storms, *Philos. Trans. R. Soc. London A*, *255*, 505–584.

Pierson, W. L., Jr., and L. Moskowitz (1964), A proposed spectral form for fully developed wind seas based on similarity theory of S. A. Kitaigorodskii, *J. Geophys. Res.*, *69*, 5182–5190.

Withers, M., R. Aster, C. Young, and E. Chael (1996), High-frequency analysis of seismic background noise and signal-to-noise ratio near Datil, New Mexico, *Bull. Seismol. Soc. Am.*, *86*, 1507–1515.

R. C. Aster, Department of Earth and Environmental Science, New Mexico Institute of Mining and Technology, Socorro, NM 87801, USA. (aster@ees.nmt.edu)

P. D. Bromirski, Integrative Oceanography Division 0209, Scripps Institution of Oceanography, 9500 Gilman Dr., La Jolla, CA 92093, USA.

D. E. McNamara, U.S. Geological Survey, Box 25048, Stop 966, Denver Federal Center, Denver, CO 80225, USA.